Developmental Biology 447 (2019) 157–169

Contents lists available at ScienceDirect

Developmental Biology

journal homepage: www.elsevier.com/locate/developmentalbiology

Epithelial *DNA methyltransferase-1* regulates cell survival, growth and maturation in developing prostatic buds

Diya B. Joseph[a], Anoop S. Chandrashekar[a], Lisa L. Abler[a], Li-Fang Chu[b,c], James A. Thomson[b,c], Chad M. Vezina[a,*,1]

[a] Department of Comparative Biosciences, School of Veterinary Medicine, University of Wisconsin-Madison, Madison, WI 53706, USA
[b] Morgridge Institute for Research, Madison, WI 53715, USA
[c] Department of Cell and Regenerative Biology, University of Wisconsin School of Medicine and Public Health, Madison, WI 53707-7365, USA

ARTICLE INFO

Keywords:
Prostate
DNMT1
P53
Urethra
Epigenetics
Budding

ABSTRACT

DNA methyltransferase 1 (DNMT1) is required for embryogenesis but roles in late forming organ systems including the prostate, which emerges from the urethral epithelium, have not been fully examined. We used a targeted genetic approach involving a *Shhcre* recombinase to demonstrate requirement of epithelial DNA methyltransferase-1 (*Dnmt1*) in mouse prostate morphogenesis. *Dnmt1* mutant urethral cells exhibit DNA hypomethylation, DNA damage, p53 accumulation and undergo cell cycle arrest and apoptosis. Urethral epithelial cells are disorganized in *Dnmt1* mutants, leading to impaired prostate growth and maturation and failed glandular development. We evaluated oriented cell division as a mechanism of bud elongation and widening by demonstrating that mitotic spindle axes typically form parallel or perpendicular to prostatic bud elongation axes. We then deployed a Shh^{creERT} allele to delete *Dnmt1* from a subset of urethral epithelial cells, creating mosaic mutants with which to interrogate the requirement for cell division in specific prostatic bud epithelial populations. DNMT1- cell distribution within prostatic buds is not random as would be expected in a process where DNMT1 was not required. Instead, replication competent DNMT1 + cells primarily accumulate in prostatic bud margins and tips while replication impeded DNMT1- cells accumulate in prostatic bud cores. Together, these results highlight the role of DNMT1 in regulating epithelial bud formation by maintaining cell cycle progression and survival of rapidly dividing urethral epithelial cells, which can be extended to the study of other developing epithelial organs. In addition, our results show that prostatic buds consist of two epithelial cell populations with distinct molecular and functional characteristics that could potentially contribute to specialized lineages in the adult prostate.

1. Introduction

Prostatic buds arise from the urethral epithelium in response to androgen signaling in adjacent mesenchyme. Coordinated epithelial-mesenchymal interactions guide morphogenesis in the developing prostate as in other budding organ systems. While morphogens, growth factors and their receptors have been a major focus of mechanistic studies, few studies have examined how epigenetic processes engage in morphogenesis. DNA methyltransferase-1 (DNMT1) carries out cytosine methylation of unmethylated daughter strands in newly replicated DNA (Monk et al., 1987; Reik et al., 2001). *Dnmt1* knockout mice die at mid-gestation, highlighting a critical role in early embryonic development (Li et al., 1992). We previously reported that *Dnmt1* expression domains change synchronously with prostatic bud specification and initiation. *Dnmt1* expression is widespread in urethral epithelium and stroma prior to bud formation at E16.5 and restricts to highly proliferative basal epithelial cells during prostatic bud specification and initiation (Keil et al., 2013). DNA methylation regulates prostate morphogenesis through diverse molecular processes including epithelial adhesion and androgen receptor signaling. We found that DNA methylation decreases prior to prostatic bud initiation at the androgen receptor (*Ar*) locus and increases during prostatic bud outgrowth at the E-cadherin (*Cdh1*) locus. By selectively inhibiting DNA methylation with the DNMT1 inhibitor 5-aza-2′-deoxycytidine

* Corresponding author.
E-mail address: chad.vezina@wisc.edu (C.M. Vezina).
[1] Lead Contact.

https://doi.org/10.1016/j.ydbio.2019.01.011
Received 15 November 2018; Received in revised form 17 December 2018; Accepted 14 January 2019
Available online 16 January 2019
0012-1606/

(5AzadC) at key developmental stages, we either increased *Ar* abundance and accelerated prostatic bud formation or increased *Cdh1* abundance and interfered with bud outgrowth (Keil et al., 2014a, 2014b).

Our previous findings revealed essential roles of DNA methylation in prostatic bud morphogenesis, but we did not pinpoint whether prostatic bud formation requires DNMT1 in the mesenchyme or epithelium because it was not possible to deliver 5AzadC in a cell-specific manner. We were also unable to examine the requirement for DNMT1 in vivo because 5AzadC is a lethal teratogen (Bulut et al., 1999) which interacts non-specifically with other epigenetic processes (Wozniak et al., 2007), and interferes with testicular development and androgen synthesis (Choi et al., 2013; Cisneros and Branch, 2003).

To circumvent limitations of pharmacological DNMT1 inhibition, we employed targeted genetic approaches to delete *Dnmt1* in the urethral epithelium that gives rise to prostatic buds. Targeted genetic approaches have been used previously to interrogate the role of DNMT1 in the developing bladder (Joseph et al., 2018), intestine (Elliott et al., 2015), retina (Nasonkin et al., 2013) and pancreas (Georgia et al., 2013), but the prostate has not been studied in this context. We used a *Shhcre* driver (Harfe et al., 2004) to conditionally delete *Dnmt1* across urethral epithelium from which prostatic buds emerge (c*Dnmt1*KOs) and discovered that DNMT1 is required for prostatic bud formation and elongation and maintains urethral epithelial cell integrity, cell cycle progression and survival. DNMT1 depleted cells undergo G2/M cell cycle arrest and apoptosis. c*Dnmt1*KO urethras, rescued from embryos and grafted under the kidney capsule for continued development, are devoid of mature prostate glands. These findings establish a critical role for DNMT1 in regulating prostatic budding by maintaining survival of urethral epithelial cells from which prostatic buds emerge.

The exact identity of urethral epithelial cells that give rise to prostatic buds remains unclear. It was initially believed that a single urethral epithelial cell type, characterized by expression of basal epithelial cell markers KRT14 and TRP63, gave rise to prostatic bud and ductal epithelium (Kurita et al., 2004; Signoretti and Loda, 2006; Signoretti et al., 2005). Recent results indicate these factors are not ubiquitous across the prostatic bud. KRT14 and TRP63 are more abundant in epithelial cells of the lateral and distal portions of prostatic buds (margin cells) than inner (core) prostatic bud epithelial cells (Abler et al., 2011a; Mehta et al., 2013). Whether molecular differences extend to functional or physiological differences between prostatic bud epithelial cell populations has not been examined. A greater understanding of these molecular differences and how it is established could resolve which developmental processes (oriented cell division, convergent extension, collective cell migration, epithelial-to-mesenchymal cell transition) underlie prostatic bud elongation. In this study, we show that prostatic bud epithelial cells divide parallel and perpendicular to the bud axis to elongate and widen prostatic buds.

Having demonstrated oriented cell division in prostatic buds and the requirement for DNMT1 in cell survival, we leveraged our new findings to pinpoint the contribution of cell proliferation to prostatic bud elongation. Specifically, we used *Dnmt1* deletion as tool to determine whether DNA methylation-dependent cell proliferation is equally required in all epithelial cells within the prostatic bud. The approach involved a $Shh^{creErt2}$ driver to achieve *Dnmt1* inactivation in a subset (mosaic) of urethral epithelium (i*Dnmt1*LOFs). Though prostatic bud development proceeds normally in i*Dnmt1*LOF mice, DNMT1- cells are not randomly distributed in prostatic buds. Replication competent DNMT1 + cells accumulate preferentially in prostatic bud margins and tips while DNMT1- replication impeded cells are excluded from bud margins and tips, accumulating instead in prostatic bud cores. These results are consistent with differing cell proliferation requirements in prostatic bud margin versus core epithelial cells and allow for the possibility that prostatic bud core cells arise from a non-proliferative mechanism such as cell migration.

2. Material and methods

2.1. Animals

Mice were housed as previously described (Mehta et al., 2011). All procedures performed on mice were approved by the University of Wisconsin-Madison Animal Care and Use Committee and were carried out in accordance with the Guide for the Care and Use of Laboratory Animals. All embryos used in this study were obtained from timed matings. Mice carrying the *Dnmt1Flox* allele (B6.129S4-$Dnmt1^{tm2Jae/Mmucd}$) were from the Mutant Mouse Research and Resource Centers at the University of California, Davis (MMRRC, 014114-UCD). Genotyping for the *Dnmt1Flox* allele was carried out as described previously (Jackson-Grusby et al., 2001). Mice carrying the $Shh^{creErt2}$ allele (B6.129S6-$Shh^{tm2(cre/ERT2)Cjt/J}$, The Jackson Laboratory, 005623) and the *Shhcre* allele (B6. Cg-$Shh^{tm1(EGFP/cre)Cjt/J}$, The Jackson Laboratory, 005622) were genotyped as described previously (Harfe et al., 2004; Mehta et al., 2013). Mice carrying the Cre inducible *R26R-LacZ* reporter allele (B6;129S4-*Gt(ROSA)* $26^{Sortm1Sor/J}$, The Jackson Laboratory, 003309) were genotyped as described previously (Soriano, 1999). Mice carrying the *R26R-EYFP* reporter allele (B6.129 ×1-$Gt(ROSA)26^{Sortm1(EYFP)Cos/J}$, The Jackson Laboratory, 006148) were genotyped as previously described (Srinivas et al., 2001). *Dnmt1Flox* mice were bred to mice carrying either the *R26R-LacZ* or *R26R-EYFP* alleles to obtain *Dnmt1Flox/Flox; R26R/R26R* females. These females were used for timed matings with *Shhcre/+ ; Dnmt1Flox/+* or *ShhcreErt2/+ ; Dnmt1Flox/+* males. Dams were euthanized by CO_2 asphyxiation to harvest embryos. Of the resulting male offspring, *cre/+ ; Dnmt1Flox/+ ; R26R/+* embryos were used as controls and compared to litter mates of the genotype *cre/+ ; Dnmt1Flox/Flox; R26R/+* . Wildtype C57Bl6/J or CD-1 mice were obtained from the Jackson laboratory or Charles River laboratories respectively.

2.2. Tamoxifen administration

Pregnant dams were dosed intra-peritoneally with sterile corn oil (2.5 ml/kg) containing 10% ethanol, tamoxifen (200 mg/kg mouse weight, Sigma #T56482, St. Louis MO) and progesterone (75 mg/kg mouse weight, Watson #NDC0591-3128-79, Corona CA) on embryonic day 9.5 to activate Cre recombinase in embryos carrying the $Shh^{creErt2}$ allele. Dams were euthanized by CO_2 asphyxiation and embryos were collected at embryonic day 18.5.

2.3. Renal grafting

Embryonic day 18.5 urogenital sinuses were placed under the renal capsule of 6–12 week intact male athymic *nu/nu* mice (The Jackson Laboratory, 002019). Grafts were grown for 1 month before tissues were collected.

2.4. Fluorescent Immunohistochemistry

Fluorescent immunohistochemistry was performed as described previously (Abler et al., 2011a). Dissected tissues were fixed overnight in 4% paraformaldehyde and processed to obtain paraffin sections. 5 μm paraffin sections were deparaffinized in xylene and hydrated through a series of ethanol washes. Heat mediated antigen retrieval was performed by boiling slides in 10 mM sodium citrate (pH 6.0) for 20 mins in a conventional microwave oven. Tissues were washed with a solution containing 25 mM Tris-HCl, pH 7.5, 140 mM NaCl, 2.7 mM KCl, and 0.1% Tween-20 (TBSTw) and non-specific binding sites were blocked for 1 h in TBSTw containing 1% Blocking Reagent (Roche Diagnostics, Indianapolis, IN), 5% normal goat sera, and 1% bovine serum albumin fraction 5 (RGBTw). Tissues were incubated overnight at 4 °C with primary antibodies diluted in

RGBTw. Following primary antibody incubation, tissues were washed several times in TBSTw and incubated with secondary antibodies diluted in RGBTw for 1 h at room temperature. Tissues were washed in TBSTw and labeled with 4′,6-diamidino-2-phenylindole, dilactate (DAPI) to visualize cell nuclei and mounted in phosphate buffered saline containing 80% glycerol and 0.2% n-propyl gallate. Images were obtained using a Leica SP8 Confocal Microscope fitted with a 20X oil immersion objective (HC PL Apo CS2 NA = 0.75) (Leica, Wetzlar, Germany) or a Nikon Eclipse E600 compound microscope fitted with 10 × (Plan Fluor NA = 0.30) and 20X objectives (Plan Fluor NA = 0.50) (Nikon Instruments Inc., Tokyo, Japan). Sections from both experimental groups were imaged using the same exposure settings or laser power for a given antibody combination. The tile-scanning function was used to obtain images of entire tissue sections containing the urethra to reduce sampling bias. For primary and secondary antibody information see Key resource table.

2.5. EdU Proliferation assay

5-ethynyl-2′-deoxyuridine (Thermo Fisher Cat #A10044–50 mg) was dissolved in sterile saline to a concentration of 1 mg/ml. Timed pregnant females were dosed intraperitoneally at 5 mg EdU/kg body weight two hours prior to euthanasia to label S phase cells in embryos. Tissue sections from EdU dosed embryos were labeled using the Click-iT EdU Alexa Fluor 488 Imaging kit (Thermo Fisher Cat #C10337).

2.6. Mitotic spindle angle measurements

Mitotic spindles in tissue sections were labeled using antibodies to Gamma tubulin (Abcam #ab11317). Spindle angles were computed with respect to a tangent drawn to the closest bud edge using *ImageJ v 1.51k* as previously described (Feng et al., 2013). Spindle angles were binned

Reagent or resource	Source	Identifier
Antibodies		
Mouse monoclonal anti– 5 methylcytosine	Abcam	Cat#ab10805; RRID:AB_442823
Chicken polyclonal anti-LacZ	Abcam	Cat# ab9361, RRID:AB_307210
Chicken polyclonal anti-GFP	Abcam	Cat#ab13970; RRID:AB_300798
Rabbit polyclonal anti-Ki67	Abcam	Cat#ab15580; RRID:AB_443209
Rabbit polyclonal anti-Gamma Tubulin	Abcam	Cat# ab11317; RRID:AB_297921
Rabbit polyclonal anti-PAX2	Covance	Cat#PRB-276P-200; RRID:AB_291611
Mouse monoclonal anti-FOXA1	Millipore	Cat#05–1466; RRID:AB_1977191
Chicken polyclonal anti-KRT5	Biolegend	Cat#905901; RRID: AB_2565054
Rabbit monoclonal anti– 5 methylcytosine	Cell Signaling	Cat#28692
Rabbit monoclonal anti-DNMT1	Cell Signaling	Cat#D63A6; RRID:AB_10828695
Rabbit monoclonal anti-CDH1	Cell Signaling	Cat#3195 S
Rabbit polyclonal anti-Histone H2AX (phospho Ser139)	Cell Signaling	Cat#2577; RRID:AB_2118011
Mouse monoclonal anti-p53 (phospho Ser15) 16G8	Cell Signaling	Cat#9286; RRID:AB_331741
Rabbit monoclonal anti-Cleaved Casp3 (Asp 175)	Cell Signaling	Cat#9664; RRID:AB_2070042
Rabbit polyclonal anti-Phospho-Histone H3 (Ser10)	Cell Signaling	Cat#9701; RRID:AB_331535
Mouse monoclonal anti-CDH1	BD Transduction Labs	Cat#610181; RRID:AB_397580
Mouse monoclonal anti-ZO1	Thermo Fisher Scientific	Cat#33–9100; RRID:AB_2533147
Mouse monoclonal anti-KRT14	Thermo Fisher Scientific	Cat# MS-115-P0, RRID:AB_63786
Goat polyclonal anti-Chicken Alexa488 conjugated	Jackson Immunoresearch	Cat#103-545-155; RRID:AB_2337390
Goat polyclonal anti-Mouse Alexa488 conjugated	Jackson Immunoresearch	Cat# 115-547-003; RRID:AB_2338869
Goat polyclonal anti-Rabbit Alexa488 conjugated	Jackson Immunoresearch	Cat# 111-547-003; RRID:AB_2338058
Goat polyclonal anti-Mouse Alexa594 conjugated	Jackson Immunoresearch	Cat# 115-585-062; RRID:AB_2338876
Goat polyclonal anti-Rabbit Alexa594 conjugated	Jackson Immunoresearch	Cat# 111-586-045; RRID:AB_2338067
Sheep polyclonal anti-Digoxygenin Alkaline phosphatase conjugated	Roche	Cat#11093274910; RRID:AB_514497
Chemicals, Peptides, and Recombinant Proteins		
Tamoxifen, free base	Sigma Aldrich	T5648; CAS: 10540–29-1
5-ethynyl– 2′-deoxyuridine (EdU)	Thermo Fisher	A10044
Critical Commercial Assays		
Click-iT® EdU Alexa Fluor® 488 Imaging Kit	Thermo Fisher	C10337
Deposited Data		
RNA-Seq data	This paper	GEO: GSE121086
Experimental Models: Organisms/Strains		
Mouse: B6.129S4-*Dnmt1*$^{tm2Jae/Mmucd}$	MMRRC, UC Davis	Stock#014114-UCD; RRID: MMRRC_014114-UCD

Mouse: B6. Cg*Shh*$^{tm1(EGFP/cre)Cjt/J}$	Jackson Laboratory	Stock#005622; RRID: IMSR_JAX:005622
Mouse: B6.129S4-*Gt(ROSA)26*$^{Sortm1Sor/J}$	Jackson Laboratory	Stock#003309; RRID: IMSR_JAX:003309
Mouse: B6.129 × 1-*Gt(ROSA)26*$^{Sortm1(EYFP)Cos/J}$	Jackson Laboratory	Stock#006148; RRID: IMSR_JAX:006148
Mouse: B6.129S6-*Shh*$^{tm2(cre/ERT2)Cjt}$/J	Jackson Laboratory	Stock#005623; RRID: IMSR_JAX:005623
Mouse: CD– 1 IGS mouse (wildtype)	Charles Rives	Stock#022
Mouse: C57BL/6	Jackson Laboratory	Stock#000664, RRID: IMSR_JAX:000664
Mouse: Athymic nude nu/nu	Jackson Laboratory	Stock#002019
Oligonucleotides		
Primer: *Cdkn1a* Forward 5′- ATACCGTGGGTGTCAAAGCAC– 3′	This paper	N/A
Primer: *Cdkn1a* Reverse 5′- ACAGGGAGGGAGCCACAATAC– 3′	This paper	N/A
Primer: *Ppia* Forward 5′- TCTCTCCGTAGATGGACCTG– 3′	This paper	(Keil et al., 2014)
Primer: *Ppia* Reverse 5′- ATCACGGCCGATGACGAGCC– 3′	This paper	(Keil et al., 2014)
Mouse *Nkx3–1* ISH probe Forward primer 5′-CAGTGGCTGATGTCAAGG-3′	This paper	(Abler et al., 2011)
Mouse *Nkx3–1* ISH probe Reverse primer 5′-CGATGTTAATACGACTCACTATAGGGCTAAGCAGGAAGGGCAGGAG-3′ (T7 binding site underlined)	This paper	(Abler et al., 2011)
Nkx3–1 ISH probe binding site NM_010921.3	This paper	(Abler et al., 2011)
Software and Algorithms		
ImageJ	imagej.nih.gov	Version 1.51k
R for Windows	cran.r-project.org	Version 3.3.1
Adobe Illustrator	adobe.com	CC2017
Adobe Photoshop	adobe.com	CC2017
DESeq. 2 package	bioconductor.org	(Love et al., 2014)

into 3 categories: 0–30 degrees (parallel to axis of bud extension), 30–60 degrees (random) and 60–90 degrees (perpendicular to axis of bud extension).

2.7. RNA in situ hybridization

In situ hybridization for whole tissues was carried out as described previously (Abler et al., 2011b; Keil et al., 2012a). For in situ hybridization on tissue sections, lower urinary tracts fixed overnight in phosphate buffered saline containing 4% paraformaldehyde were embedded in OCT embedding medium and cut into 10-micron sections before probe hybridization. Sequences for primers used in riboprobe synthesis are as follows: Mouse *Nkx3-1* 5′- CAGTGGCTGATGTCA AGG-3′ and 5′-CGATGTTAATACGACTCACTATAGGGCTAAGCAGGA AGGGCAGGAG-3′. After completion of the colorimetric reaction, tissues were fixed overnight in phosphate buffered saline containing 4% paraformaldehyde before imaging using a Nikon Eclipse 80i compound microscope or an Olympus SZX10 dissecting microscope.

2.8. Hematoxylin-eosin staining

5-micron paraffin sections were washed in xylene and rehydrated through a series of graded ethanol washes. Slides were washed in water, Hematoxylin QS (Vector Laboratories, Burlingame, CA, US) was added dropwise to cover tissue sections and tissues were stained for 8 min. Slides were washed in tap water and phosphate buffered saline to develop stain. Slides were then washed in a 50% ethanol solution followed by a 75% ethanol solution. Slides were incubated in eosin working solution (0.25% eosin, 60% ethanol, 0.5% glacial acetic acid) for 2 min and dehydrated through a series of graded ethanol washes. Slides were washed in xylene and mounted with Richard-Allan Scientific™ Mounting Medium (Thermo Fisher Scientific, Waltham, MA, USA) before coverslips were applied. Images were obtained using a Nikon eclipse 80i compound microscope.

2.9. Whole-mount tissue staining

Lower urinary tract tissue was harvested from E18.5 embryos. Tissues were briefly washed in cold phosphate buffered saline and fixed in 4% paraformaldehyde solution for 20 mins on ice. Tissues were washed in 25 mM Tris-HCl, pH 7.5, 140 mM NaCl, 2.7 mM KCl, and 0.1% Triton-X100 (TBSTx). Tissues were then digested with 1 mg/ml Collagenase from *Clostridium histolyticum*, washed and post-fixed in 4% paraformaldehyde for 20 mins. Tissues were washed and blocked for 1 h in TBSTx containing 1% Blocking Reagent (Roche Diagnostics, Indianapolis, IN), 5% normal goat sera, and 1% bovine serum albumin fraction 5 (RGBTx) with 0.5% Triton X-100% and 1% dimethyl sulfoxide. After blocking, tissues were incubated in RGBTx containing primary antibodies overnight at room temperature. Tissues were washed 5 times for 1 h in TBSTx and incubated with secondary antibodies diluted in RGBTx (overnight at 4 °C). Tissues were washed 5 times for 1 h each in TBSTx and cleared in Citifluor (Electron Microscopy Sciences). Images were obtained using a Leica SP8 Confocal Microscope.

2.10. RNA-seq

Urethral epithelia were isolated by trypsin digestion as described previously (Cunha and Baskin, 2016). Dissected tissues were placed directly into RLT Plus lysis buffer (Qiagen) for later processing. Dissected tissues from multiple embryos were pooled into one lysate. Total RNA was purified from the RLT Plus lysates using the RNeasy Plus Micro Kit (Qiagen) according to manufacturer's instructions. For constructing the RNA-Seq library, total RNA from each batch of samples (using an input of ~100 ng total RNA) was used following the LM-seq protocol (Hou et al., 2015). The reads generated from the Illumina HiSeq. 3000 (69 cycles of insert read and 10 cycles of index read) were processed with CASAVA basecalling software (Illumina). The demultiplexing step allotted approximately 124.7 million total

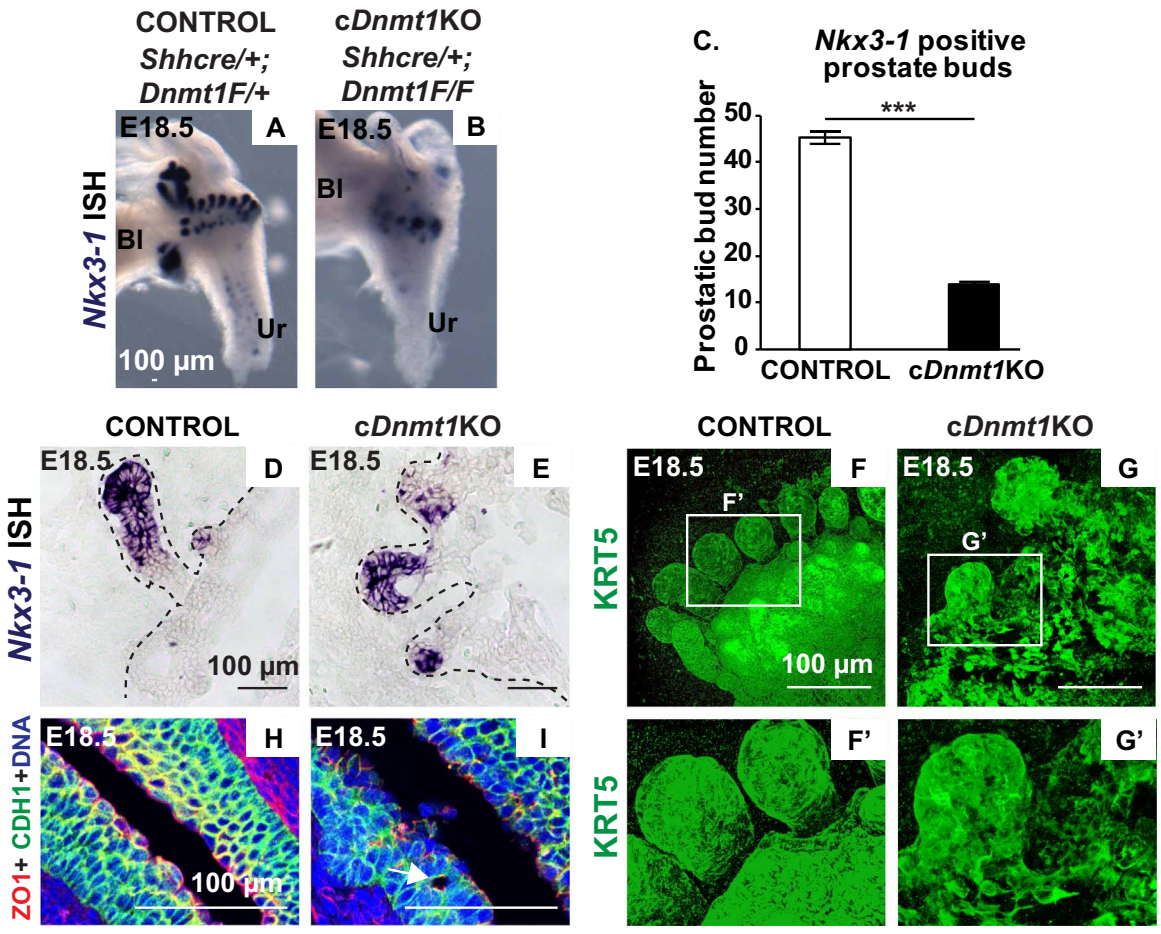

Fig. 1. DNMT1 is required for prostatic bud formation and maintains epithelial organization in the urethra. E18.5 control and c*Dnmt1*KO urethras were (A–B) labeled with an *Nkx3-1* riboprobe to visualize prostatic buds (purple) and (C) buds were quantified. (D–E) 10-micron frozen sections from E18.5 control and c*Dnmt1*KO urethras were labeled with an *Nkx3-1* riboprobe (purple) to visualize the cellular organization of prostatic buds. Black dashed lines indicate the epithelial-mesenchymal interface. (F–G) E18.5 control and c*Dnmt1*KO male urethras were stained in whole-mount with an antibody against KRT5 (in green) to visualize the basal epithelial surface of the urethra and prostatic buds. (F') and (G') show magnified regions from (F) and (G) respectively. (H–I) E18.5 urethral sections were labeled with antibodies against ZO-1 (in red, labels tight junctions) and CDH1 (in green, labels epithelium). The white arrow indicates an acellular hole with apical ZO-1 staining in a c*Dnmt1*KO urethra. DAPI staining is shown in blue. Scale bar is 100 µm. Graphical results are the mean ± SEM of at least three mice per group. p-values indicate significant differences (*** $p < 0.001$) between groups based on Student's *t*-test. Abbreviations are Ur: Urethra, Bl: Bladder.

reads across the all the samples, ranging from ~0.7 million to ~18.9 million reads assigned per sample. Reads were mapped to Mus musculus reference mm10 assembly with an average of ~66% mapping rate using Bowtie (Langmead et al., 2009), and gene expression estimates were obtained using RSEM (Li and Dewey, 2011). Differentially expressed genes were identified using the *DESeq. 2* package (Love et al., 2014). Independent filtering was performed to eliminate genes with less than 10 reads in all samples combined. Genes with adjusted p-value or False discovery rate (FDR) < 0.05 were categorized as differentially expressed. Gene Ontology enrichment analysis for biological processes was conducted using WebGestalt (Wang et al., 2017). RNA-Seq data was deposited in Gene Expression Omnibus (www.ncbi.nlm.nih.gov/geo/) Accession number: GSE121086.

2.11. Real-time quantitative PCR

Quantitative PCR was carried out as previously described (Keil et al., 2014a, 2012b). Relative mRNA abundance was determined using the ΔCt method (Yuan et al., 2006) and normalized to the abundance of housekeeping gene *Ppia*. Urethral tissue from four embryos was used for analysis. Primers sequences are provided in the Key resource table.

2.12. Statistical analysis

Statistical analysis was conducted using *R* version 3.3.1. Two tailed Student's *t*-test was performed on untransformed data that passed the Bartlett's test for homogeneity of variance. P values less than 0.05 were considered statistically significant (* $p < 0.05$, ** $p < 0.01$, *** $p < 0.001$). Results are presented as mean ± standard error of mean (SEM) from at least 3 litter independent male embryos per genotype.

3. Results

3.1. Epithelial DNMT1 is required for prostatic bud formation

We used *Shhcre* and *Dnmt1Flox* alleles to test whether *Dnmt1* deletion from urethral epithelium reduces prostatic budding. The *Shhcre* allele expresses Cre recombinase throughout the urethral epithelium starting as early as E10.5, which is prior to the onset of prostatic bud formation at E16.5 (Seifert et al., 2008). We compared embryos carrying one copy of the *Shhcre* allele and one copy of the *Dnmt1Flox* allele (control) to those carrying one copy of the *Shhcre* allele and two copies of the *Dnmt1Flox* allele (c*Dnmt1*KO). Cre inducible R26R-LacZ or R26R-EYFP alleles were also incorporated to visualize Cre-mediated recombination. c*Dnmt1*KO newborns do not survive more than a few minutes, are cyanotic and have severely hypoplastic lungs compared to controls (Joseph et al., 2018).

DNMT1 protein is expressed throughout the urethral epithelium with the highest expression in prostatic buds. Abundant DNMT1 expression in rapidly dividing prostatic bud cells maintains 5mC levels

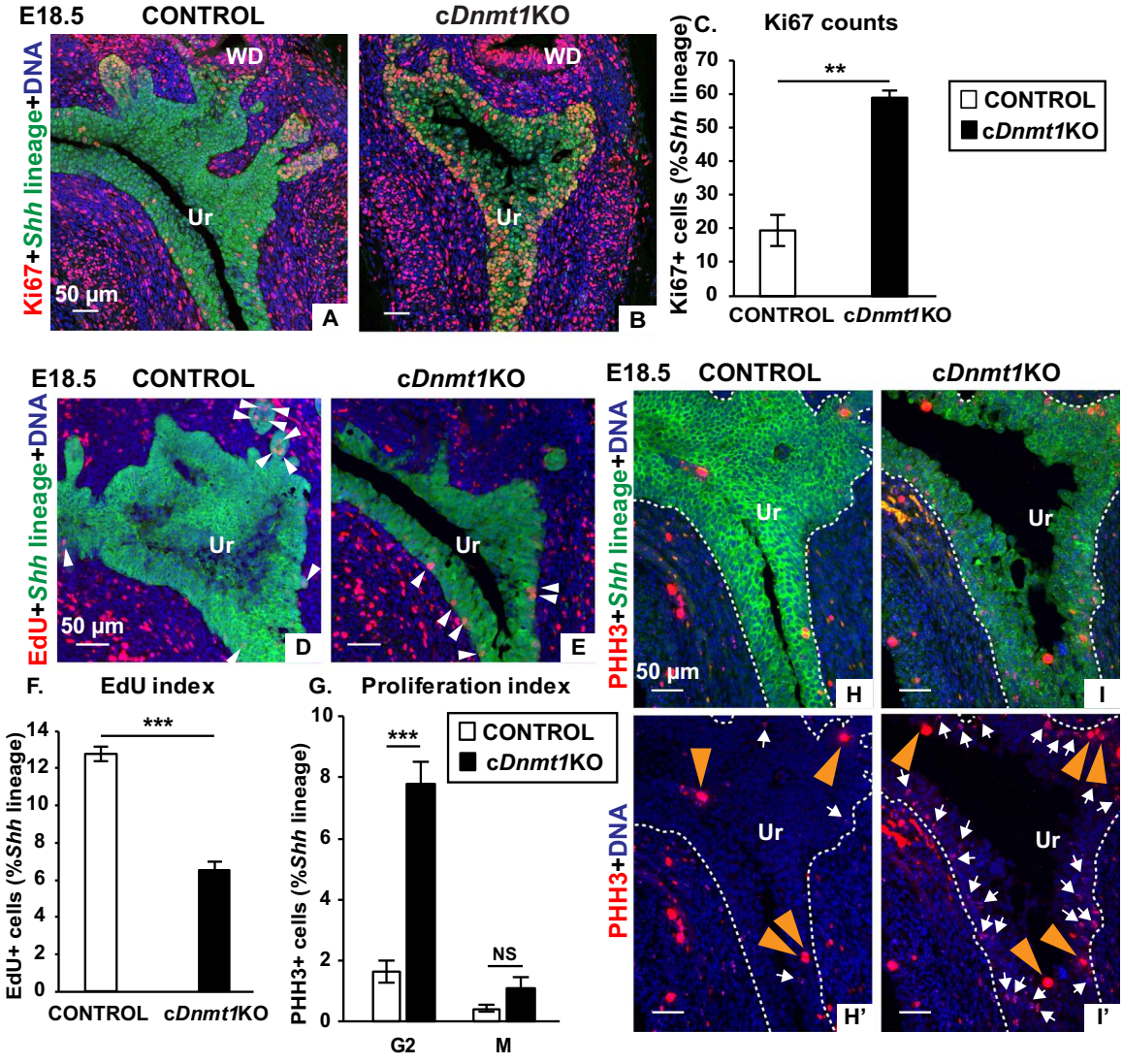

Fig. 2. DNMT1 is required for normal cell cycle progression in urethral and prostatic epithelial cells. (A–B) E18.5 urethra sections were labeled with antibodies against Ki67 (red, labels proliferating cells) and EYFP (green, labels *Shh* lineage epithelium). (C) Ki67 positive cells as a percentage of total urethral *Shh* lineage cells was determined. (D-E) E18.5 urethra sections were labeled for EdU (in red, labels S-phase cells) and EYFP (in green, labels *Shh* lineage epithelium). White arrowheads indicate EdU positive cells. (F) EdU positive cells as a percentage of total urethral *Shh* lineage cells was determined. (G) G2 and M phase cells as a percentage of total urethral *Shh* lineage cells was determined (H-I) E18.5 urethra sections were labeled with antibodies against Phospho-histone H3 Ser10 (PHH3 in red, labels cells in the G2 and M phase) and EYFP (in green, labels *Shh* lineage epithelium). (H′) and (I′) show (H) and (I) with the green channel excluded. G2 phase cells have speckled nuclear staining of PHH3 and are indicated by white arrows. M phase cells have bright, uniform nuclear staining for PHH3 and are indicated by orange arrowheads. White dashed lines indicate the epithelial-mesenchymal interface. DAPI staining is shown in blue. Scale bar is 50 μm. Graphical results are the mean ± SEM of at least three mice per group. p-values indicate significant differences (** $p < 0.01$, *** $p < 0.001$) between groups based on Student's unpaired *t*-test. NS: Not significant $p > 0.05$. Abbreviations are WD: Wolffian duct, Ur: Urethra.

during DNA replication by adding methyl marks to newly synthesized DNA strands. While DNMT1 protein is detectable in all urethral epithelial cells and is especially abundant in prostatic bud epithelial cells of control mice, it is undetectable in *Shh* lineage labeled c*Dnmt1*KO urethral epithelium (Fig. S1A-B). 5-methylcytosine (5mC) immunoreactivity is ubiquitous in control urethral epithelium but is undetectable in c*Dnmt1*KO urethral epithelium (Fig. S1C-D).

We tested whether prostatic bud formation is impaired by labeling isolated E18.5 urethras with an in-situ hybridization probe against NK3 homeobox 1 (*Nkx3-1*) and counting labeled buds. c*Dnmt1*KO fetuses have fewer total prostatic buds (Fig. 1A-C) and specifically fewer dorsal and anterior prostatic buds than controls (Fig. S2A). c*Dnmt1*KO prostatic buds are unusually short and wide compared to control buds (Fig. 1D-E). We also show that deleting a single *Dnmt1* allele (controls) does not affect the quantity of prostatic buds compared to *cre* negative mice (Fig. S2B), thereby validating single *Dnmt1flox* mice as appropriate controls for subsequent experiments.

To summarize, DNMT1 expression in the urethral epithelium maintains DNA methylation and is required for prostatic bud formation and elongation.

3.2. DNMT1 maintains urethral and prostatic epithelial cell organization

We performed immunolabeling with an antibody against Keratin 5 (KRT5) to assess basal epithelial surface integrity across the budding prostatic urethra. KRT5 labeling in the basal layer is discontinuous in c*Dnmt1*KO tissues while control tissues appear normal with a continuous KRT5 layer (Fig. 1F-G, Fig. S3A-B). The tight-junction protein ZO-1 was visualized as a secondary epithelial integrity measure and is

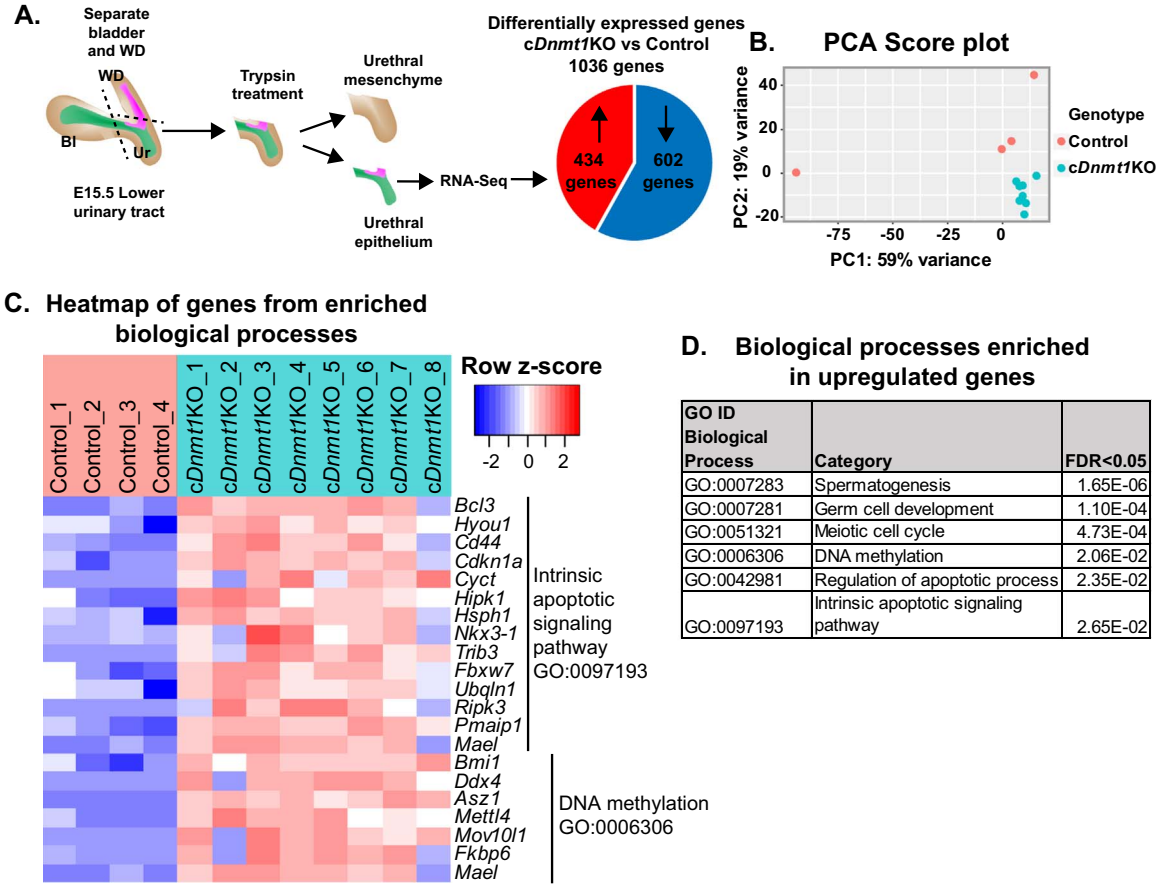

D. Biological processes enriched in upregulated genes

GO ID Biological Process	Category	FDR<0.05
GO:0007283	Spermatogenesis	1.65E-06
GO:0007281	Germ cell development	1.10E-04
GO:0051321	Meiotic cell cycle	4.73E-04
GO:0006306	DNA methylation	2.06E-02
GO:0042981	Regulation of apoptotic process	2.35E-02
GO:0097193	Intrinsic apoptotic signaling pathway	2.65E-02

Fig. 3. RNA-Seq analysis shows upregulation of p53 target genes in E15.5 c*Dnmt1*KO urethral epithelium compared to control urethral epithelium. (A) Experimental design for isolation and RNA-seq analysis of E15.5 control (n = 4 samples) and c*Dnmt1*KO urethral epithelium (n = 8 samples). (B) Principal components analysis (C) Heatmap of differentially expressed genes from enriched biological processes (D) Biological processes enriched in upregulated genes from c*Dnmt1*KO urethral epithelium. Abbreviations are WD: Wolffian duct, Ur: Urethra, Bl: Bladder, FDR: False Discovery Rate.

apically localized and continuous in control urethral epithelium but noticeably less abundant and non-apically distributed, especially around acellular holes of c*Dnmt1*KOs (Fig. 1H-I). Our results indicate that *Dnmt1* expression is required for maintaining urethral and prostatic basal epithelial organization and tight junctions.

3.3. DNMT1 is required for normal cell cycle progression in urethral and prostatic epithelium

In control urethras, DNMT1 is highly expressed in the rapidly proliferating prostatic buds but is still present in all cells of the urethral epithelium at lower, but detectable levels (Fig. S1A-B). High DNMT1 expression in prostatic buds maintains 5mC levels in the rapidly dividing cells of the prostatic buds, resulting in uniform 5mC levels throughout the urethral and prostatic epithelium. c*Dnmt1*KO urethral epithelial cells lack DNMT1 expression resulting in a drastic reduction of 5mC levels throughout the urethral epithelium. We hypothesized that the reduction in prostatic bud number in c*Dnmt1*KOs is due to proliferation defects caused by the loss of DNMT1 protein.

Although DNMT1 is preferentially localized to prostatic bud epithelium, we opted to evaluate proliferation throughout the urethral epithelium as c*Dnmt1*KO urethral epithelia show complete loss of DNMT1 protein and lack clear prostatic bud structures. We used Ki67 immunostaining to test whether a cell proliferation defect underlies impaired prostatic budding in c*Dnmt1*KOs. Nuclear Ki67 is expressed in active phases of the cell cycle. We were surprised to observe a higher percentage of Ki67 positive urethral epithelial cells in c*Dnmt1*KOs than in controls, despite reduced prostatic bud formation in c*Dnmt1*KOs. (Fig. 2A-C). To further investigate this counterintuitive finding, we decided to examine cell proliferation within the urethral epithelium in greater detail. We performed a short pulse labeling with EdU to compare S-phase cell frequencies between genotypes. Despite a greater frequency of cells entering the cycle (Ki67 +), the frequency of cells progressing to S-phase is significantly lower in c*Dnmt1*KOs compared to controls (Fig. 2D-F).

We hypothesized that cell cycle arrest at later stages promotes Ki67 + epithelial cell accumulation in c*Dnmt1*KO urethral epithelium. Phospho-histone H3 Serine 10 immunostaining was used to calculate percentages of G2 and M phase cells. G2 phase nuclei have speckled Phospho-histone H3 Serine 10 labeling while M phase nuclei are intensely and homogeneously labeled (Ozawa, 2008). The percentage of G2 phase cells is greater in c*Dnmt1*KOs than controls while the percentage of M phase cells does not differ between groups (Fig. 2G-I). Together these results indicate that c*Dnmt1*KO urethral epithelia undergo G2/M cell cycle arrest.

3.4. Loss of DNMT1 function induces DNA damage, p53 activation and apoptosis in the developing urethral and prostatic bud epithelium

We used RNA-Seq to identify molecular mechanisms contributing to G2/M cell cycle arrest in c*Dnmt1*KO urethras. Urethral epithelia were isolated at E15.5, prior to prostatic bud outgrowth. We found that 434 genes are more abundant and 602 genes less abundant in c*Dnmt1*KOs compared to controls (Fig. 3A-B). Among genes upregulated in c*Dnmt1*KOs are those involved in DNA methylation and the intrinsic apoptotic signaling pathway, including the p53 target gene cyclin dependent kinase inhibitor 1a (*Cdkn1a*, also known as p21) (Fischer, 2017) (Fig. 3C-D). *Cdkn1a* controls the G2/M cell cycle checkpoint (Agarwal et al., 1995; Niculescu et al., 1998) and its

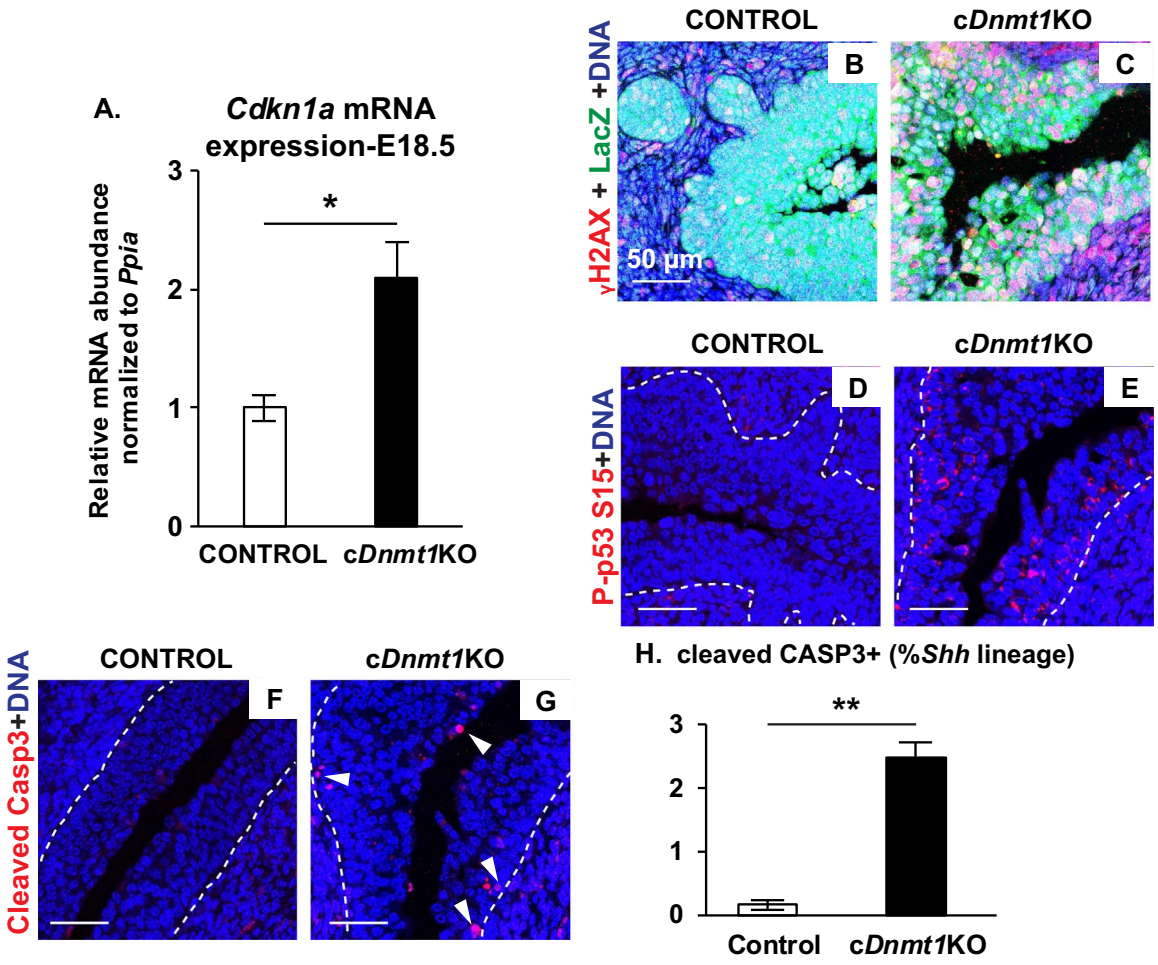

Fig. 4. Loss of DNMT1 function induces DNA damage, p53 activation and apoptosis in the developing urethral epithelium. (A) RT-PCR for *Cdkn1a* mRNA in E18.5control and c*Dnmt1*KO urethras. (B-C) E18.5 urethra sections were labeled with antibodies against Gamma-H2AX (in red, DNA damage marker) and LacZ (in green, labels *Shh* lineage epithelium). (D-E) E18.5 urethra sections were labeled with antibodies against Phospho-p53 Ser15 (in red, marks active p53). (F-G) E18.5 urethra sections were labeled with antibodies against Cleaved caspase 3 (in red, marks apoptotic cells) and EYFP (in green, labels *Shh* lineage epithelium). Green channel is excluded for ease of visualization. (H) Percentage of cleaved Caspase 3 labeled cells in the *Shh* lineage urethral epithelium. White arrowheads indicated cleaved Caspase 3 positive apoptotic cells. White dotted lines indicate epithelial-mesenchymal interface. DAPI staining is shown in blue. Scale bar is 50 μm. Graphical results are the mean ± SEM of at least three mice per group. p-values indicate significant differences (* $p < 0.05$, ** $p < 0.01$) between groups based on Student's unpaired *t*-test.

increased abundance in c*Dnmt1*KOs is consistent with G2/M arrest. We used real-time RT-PCR to confirm *Cdkn1a* mRNA is also significantly more abundant in E18.5 c*Dnmt1*KO whole prostatic urethras (epithelium+mesenchyme) than in controls (Fig. 4A).

Checkpoints prevent cells with incomplete DNA replication or DNA damage from passing incomplete or abnormal genetic material to daughter cells. In Fig. S1, we show that depleting DNMT1 diminishes 5mC. DNA hypomethylation is a trigger for the DNA damage response (Elliott et al., 2015; Palii et al., 2008), which involves activation of ATM kinases that phosphorylate and stabilize p53 to induce apoptosis (Banin et al., 1998; Georgia et al., 2013; Jackson-Grusby et al., 2001). There are more cells immune-positive for the DNA damage marker gamma H2AX in c*Dnmt1*KO urethral epithelia than in control epithelia (Fig. 4B-C) and p53 phosphorylated at Serine 15 accumulates c*Dnmt1*KO urethral epithelia (Fig. 4D-E). We also show there are more cleaved caspase 3 positive apoptotic cells in c*Dnmt1*KO urethral epithelia compared to that of controls (Fig. 4F-H). Thus, loss of DNMT1 protein leads to DNA hypomethylation, which triggers a DNA damage induced, p53-mediated apoptotic cell death pathway in c*Dnmt1*KO urethral epithelium. Collectively, we found that DNMT1 maintains DNA methylation and cell survival in urethral and prostatic bud epithelia.

3.5. DNMT1 expression is required for prostate glandular development

Prostatic gland genesis is not complete until approximately one month after birth but c*Dnmt1*KO pups die soon after birth (Joseph et al., 2018). We therefore rescued E18.5 prostatic urethras from control and c*Dnmt1*KO embryos and grafted them under the kidney capsule of intact male athymic nude mice for continued growth and development. Urethral grafts from both control and c*Dnmt1*KO tissues showed growth under the kidney capsule of athymic nude mice (Fig. 5A-B). Control grafts contain glandular structures resembling mature prostatic ducts and seminal vesicles, both with visible intraluminal secretions. Seminal vesicle tissue is expected in grafts, as the fetal material used for grafting contains seminal vesicle remnants despite removal of much of the tissue by dissection. However, c*Dnmt1*KO grafts are completely devoid of prostatic glands and instead only contain seminal vesicle tissue (Fig. 5C–D).

As further evidence for impaired prostate gland genesis in c*Dnmt1*KO mutants, we used immunohistochemistry to visualize the seminal vesicle epithelial cell marker PAX2 (Quick et al., 2010) and the endodermal marker FOXA1 (Hou et al., 2007; Taube et al., 2010). Most of control graft glandular epithelia is FOXA1 + , consistent with the

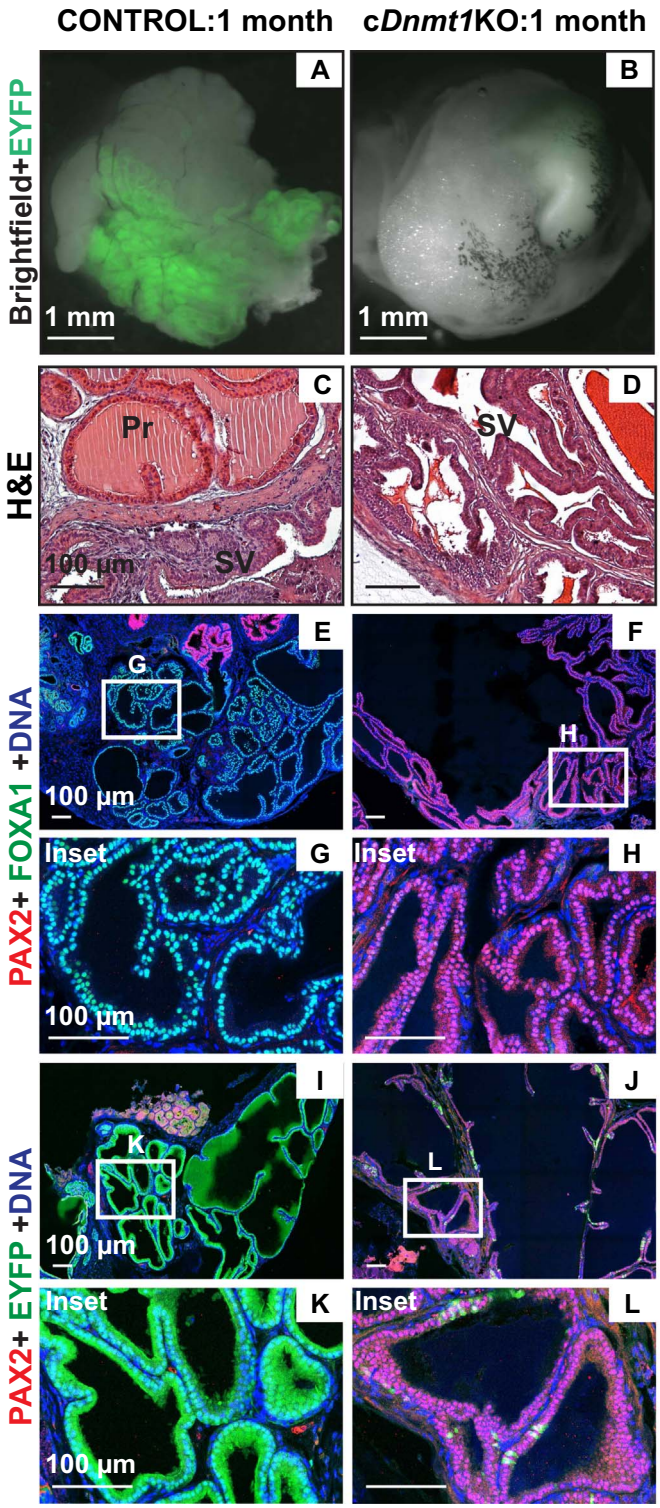

Fig. 5. DNMT1 is required for prostate gland genesis and maturation in renal grafts. (A–B) Brightfield images of renal grafts overlaid with EYFP (in green, labels *Shh* lineage epithelium). Scale bar is 1 mm. (C–D) Hematoxylin and eosin labeling of sections from renal grafts. (E-F) Sections from renal grafts were labeled with antibodies against PAX2 (in red, marks seminal vesicle epithelium) and FOXA1 (in green, marks prostate epithelium). (G) and (H) show magnified regions from (E) and (F) respectively. (I–J) Sections from renal grafts were labeled with antibodies against PAX2 (in red) and EYFP (in green). (K) and (L) show magnified regions from (I) and (J) respectively. DAPI staining is shown in blue. Scale bar is 100 µm. Images are representative of at least three grafts per genotype. Abbreviations are Pr: Prostate, SV: Seminal Vesicle.

endodermal origin of prostate tissue. In contrast, glandular epithelia in c*Dnmt1*KO grafts are devoid of FOXA1 + cells and instead harbor PAX2 + cells, consistent with seminal vesicle identity (Fig. 5E-H).

As *Shhcre* activity is absent in seminal vesicle epithelium (Seifert et al., 2008), it is expected to be negative for the Cre inducible EYFP lineage reporter. We visualized the Cre inducible EYFP reporter to test whether glandular epithelia in grafts derive from an endodermal (EYFP+, prostate) or an intermediate mesoderm origin (PAX2 +, EYFP-, ejaculatory duct and seminal vesicle). Most control graft glandular epithelial cells are EYFP+ . In contrast, c*Dnmt1*KO graft glandular epithelia are PAX2 + , EYFP-, indicating seminal vesicle epithelium (Fig. 5I-L). Although c*Dnmt1*KO grafts do not contain prostate glands, presence of mature seminal vesicle tissue confirms that grafting was successful. We conclude that DNMT1 expression in fetal prostatic epithelia is required for prostate glandular development and maturation.

3.6. Conditional DNMT1 depletion is a new strategy for examining cell replication requirements in epithelial morphogenesis

Prostatic buds have been postulated to elongate through a combination of oriented cell division and epithelial-mesenchymal transition, yet there is little direct evidence supporting either mechanism (Grant and Kyprianou, 2013). We observe that prostatic bud epithelial cells divide in an oriented manner, with mitotic spindles aligned parallel or perpendicular to the axis of bud elongation (Fig. 6A–C).

In previous figures, we show that DNMT1 depleted cells undergo cell cycle arrest and are 'replication impeded' while DNMT1 expressing cells are 'replication competent'. We leveraged these observations to examine the requirement for cell replication across prostatic bud epithelial cells. We used an inducible $Shh^{creErt2}$ allele to delete *Dnmt1* in a subset of urethral epithelial cells, creating a mosaic urethral epithelium containing replication impeded (DNMT1-) and replication competent (DNMT1 +) cells.

Embryos carrying one copy of the $Shh^{creErt2}$ allele and one copy of the *Dnmt1Flox* allele (control) were compared to embryos carrying one copy of the $Shh^{creErt2}$ allele and two copies of the *Dnmt1Flox* allele (i*Dnmt1*LOF). Pregnant dams were dosed with tamoxifen at E9.5 to activate Cre recombination in the urethral epithelium prior to the onset of prostatic budding. Prostatic bud number does not differ significantly between control and i*Dnmt1*LOF embryos (Fig. 6D-F). The Cre inducible LacZ reporter protein is expressed in a patchy pattern in i*Dnmt1*LOFs (Fig. 6G-H) and Cre recombination causes DNMT1 ablation and loss of methylation (Fig. 6I-J).

3.7. Replication competent DNMT1 + cells accumulate in prostatic bud tips while replication impeded DNMT1- cells accumulate in the prostatic bud core

Because *Dnmt1* expression in urethral epithelia is required for prostatic bud formation, we hypothesized that i*Dnmt1*LOF prostatic buds would selectively accumulate replication competent cells (DNMT1 +, 5mC+) and exclude replication impeded (DNMT1-, 5mC-) cells. Antibodies to the basal protein Keratin 14 (K14) were used to label the basal layer of urethral epithelium and developing prostatic buds. An antibody to 5mC was used to identify replication competent (5mC+) and replication impeded cells (5mC-). All cells in control urethral epithelia are 5mC+ . In i*Dnmt1*LOF urethras, the K14 + (basal layer and prostatic buds) had a higher percentage of 5mC+ cells compared to the K14- cell layer (intermediate/superficial layers) (Fig. 7A–C). This suggests that DNMT1-, 5mC- replication impeded cells are excluded from K14 + basal and prostatic bud layers.

Our results also show that 5mC- cells are not entirely excluded from prostatic buds but can instead accumulate in the core of prostatic buds

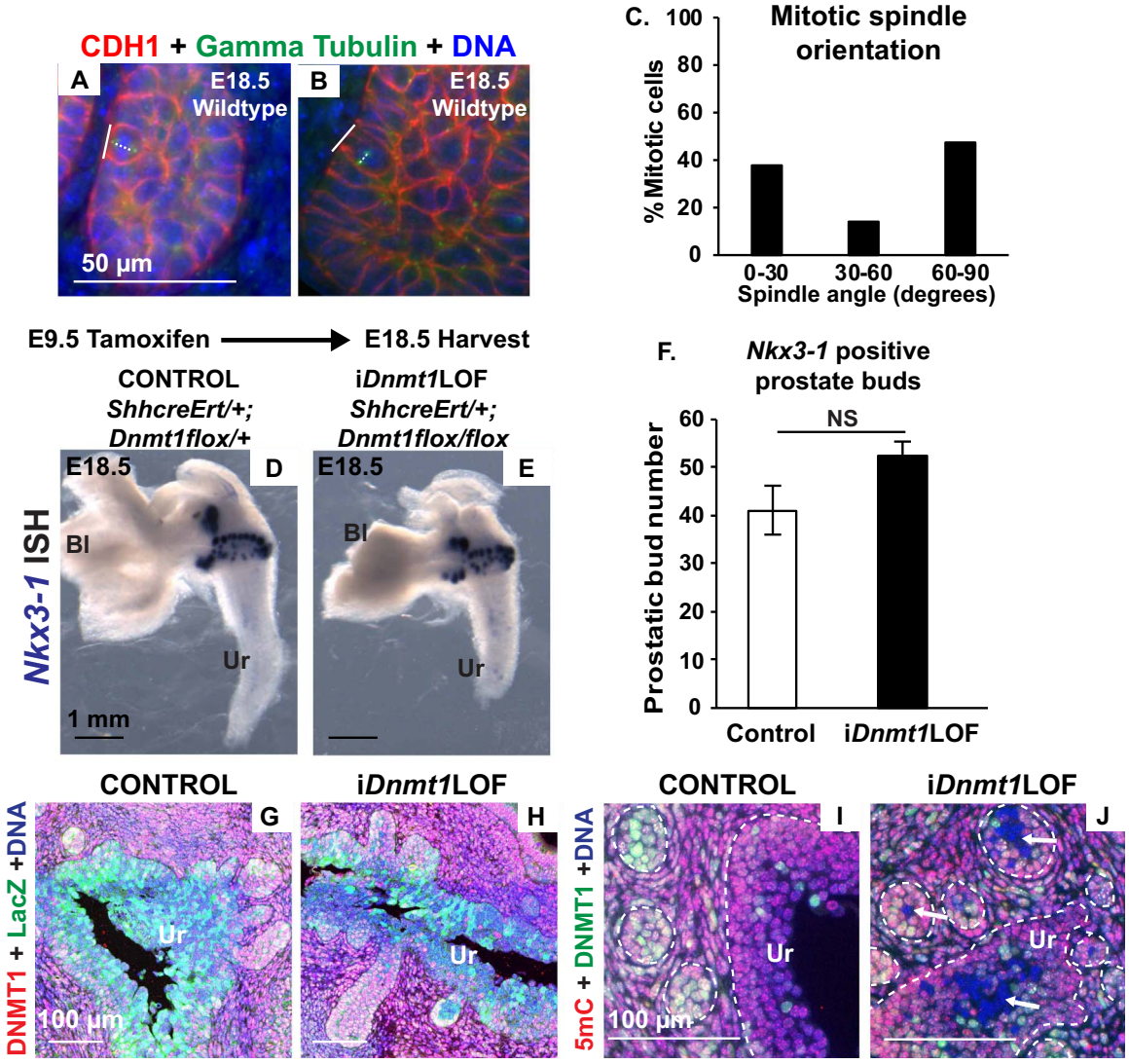

Fig. 6. Prostatic buds extend by oriented cell division but mosaic inactivation of *Dnmt1* does not affect bud formation. (A-B) Wildtype E18.5 prostatic bud sections were labeled with antibodies to Gamma tubulin (in green, labels the mitotic spindle) and CDH1 (in red, labels epithelium). The mitotic spindle axis is indicated by the white dashed line. Mitotic spindle angles are computed with respect to a tangent drawn to the nearest prostatic bud edge indicated by solid white lines. (C) Graph showing the percentage of mitotic cells (n = 21) with mitotic spindle angles that fall into the bins 0–30 degrees (parallel), 30–60 degrees (random) and 60–90 degrees (perpendicular). (D-E) E18.5control and i*Dnmt1*LOF urethras were labeled with an *Nkx3-1* riboprobe to label prostatic buds (in purple, scale bar is 1 mm) and (F) buds were quantified. Graphical results are the mean ± SEM of at least three mice per group. There were no differences between groups based on Student's unpaired *t*-test test. Not significant: NS $p > 0.05$ (G-H) E18.5 urethra sections were labeled with antibodies against DNMT1 (in red) and LacZ (in green, labels *Shh* lineage epithelium). (I-J) E18.5 urethra sections were labeled with antibodies against 5mC (in red) and DNMT1 (in green). White arrows indicate DNMT1-, 5mC- regions. White dotted lines indicate the epithelial-mesenchymal interface. Scale bar is 100 µm. Images are representative of three mice per group. DAPI staining is shown in blue. Abbreviations are Bl: Bladder, Ur: Urethra.

(Fig. 7A-C). This finding suggests there are two discrete populations of prostatic bud epithelia that contribute to prostatic bud formation by distinct mechanisms. Cells at the margins and tips of prostatic buds elongate buds axes by cell proliferation, a notion supported by the observation that complete ablation of *Dnmt1* in urethral epithelium results in fewer and shorter buds (Fig. 1A-C). However, accumulation of replication impeded DNMT1- cells in prostatic bud cores from mosaic i*Dnmt1*LOF mutants suggest these cells participate in prostatic bud growth by a proliferation independent mechanism, potentially via cell migration from the intermediate and superficial layers of the urethra.

4. Discussion

This study is the first to examine the requirement of DNMT1 in prostatic bud formation. *Nkx3-1* positive prostatic bud formation is impaired in c*Dnmt1*KO embryos, accompanied by defects in prostatic bud shape, abnormal distribution of Keratin 5 and ZO-1 indicating epithelial disorganization, and evidence of DNA damage and p53 activation. These changes are associated with increased expression of the p53 target gene *Cdkn1a*, G2/M cell cycle arrest and apoptosis. Collectively, these defects are the likely mechanism for impaired prostatic bud formation and gland genesis in c*Dnmt1*KO mutants.

In contrast to pharmacological agents that act globally, our model specifically induces cell cycle arrest in the epithelial cells of the urethra and developing prostate without affecting the surrounding mesenchyme. *Dnmt1* ablation results in a 'replication impeded' cell, which we define as cell cycle arrested. We show that *Dnmt1* depleted cells are hypomethylated, exhibit a DNA damage response and arrest in the G2 phase of the cell cycle. *Dnmt1* deleted cells can escape arrest but undergo apoptosis in the M-phase or after re-entering G1 phase (Chen et al., 2007). Because repeated cell divisions are required to deplete 5mC levels in *Dnmt1* deleted cells, our model of *Dnmt1* deletion targets fetal urethral and prostate cells that divide rapidly during organogenesis.

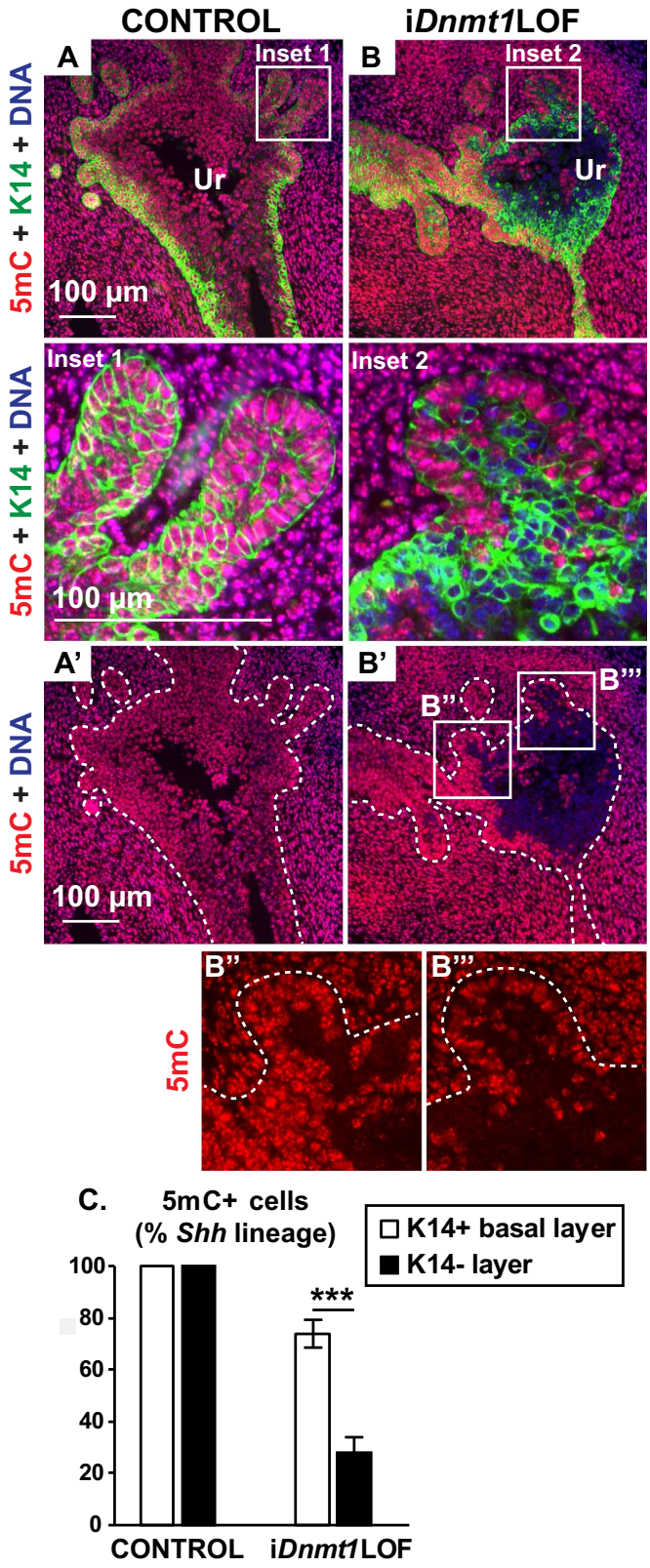

Fig. 7. Replication competent DNMT1 + cells preferentially localize to prostatic bud margins while replication impeded DNMT1- cells accumulate in prostatic bud cores. (A-B) E18.5 urethra sections were labeled with antibodies against 5mC (in red) and Keratin 14 (in green). White boxed regions from (A) and (B) are magnified in Inset 1 and Inset 2 respectively. (A') and (B') show (A) and (B) with green channel excluded. White boxed regions from (B') with blue channel excluded are shown in (B'') and (B'''). (C) The percentage of 5mC positive cells was determined as a function of all epithelial cells in either the K14 + or K14- cell layers. Graphical results are the mean ± SEM of six mice per group. p-values indicate significant differences (*** $p < 0.001$) based on Student's unpaired *t*-test. White dashed lines indicate the epithelial-mesenchymal interface. Scale bar is 100 μm. DAPI staining is shown in blue. Abbreviation Ur: Urethra.

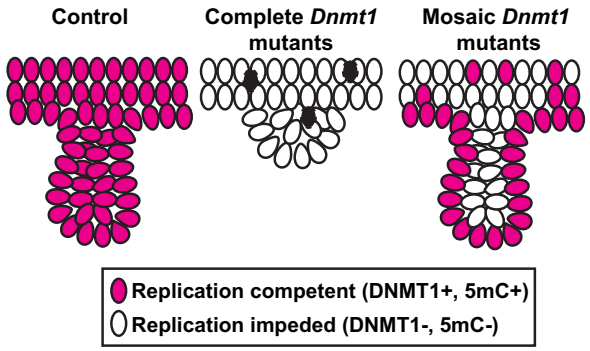

Fig. 8. Model of *Dnmt1* deletion during prostatic bud development.

We used two different strategies to delete *Dnmt1* in urethral epithelium (Fig. 8). The *Shhcre* allele confers complete recombination and widespread *Dnmt1* deletion in urethral epithelium, leading to a drastic reduction in prostatic bud number due to cell cycle arrest and apoptosis of urethral and prostate epithelial cells. In contrast, the tamoxifen inducible $Shh^{creErt2}$ allele confers mosaic inactivation of *Dnmt1*, resulting in DNMT1 + and DNMT1- cell occupation of the same tissue. Mosaic inactivation of *Dnmt1* using the $Shh^{creErt2}$ allele does not affect prostatic bud number indicating that sufficient cells escaped Cre recombination and constituted prostatic buds. Within mosaic i*Dnmt1*LOF mutants, DNMT1 + cells accumulate in the rapidly proliferating Keratin 14 + basal layer and in prostatic buds, suggesting a competitive advantage over the replication impeded DNMT1- cells and highlighting a requirement for DNMT1 in prostatic bud formation.

We used gamma tubulin immunostaining to evaluate whether prostatic bud epithelial cell division occurs in an oriented manner. We found that mitotic spindles are largely parallel and perpendicular to the long axes of prostatic buds, supporting a role for oriented cell division in prostatic bud elongation and widening. We used i*Dnmt1*LOF mice to examine whether cell division is required across all prostatic bud epithelial cells. Replication competent (DNMT1 +) cells accumulate in margins and tips of i*Dnmt1*LOF prostatic buds but replication impeded (DNMT1-) cells accumulate in prostatic bud cores. It is unlikely DNMT1- cells incorporate into buds by cell division because they are replication impeded. Their presence in buds therefore challenges the existing paradigm that prostatic buds form and elongate exclusively by a proliferation dependent mechanism and suggests that prostatic bud core cells may arise from a different mechanism. We then asked, what is the origin of prostatic bud core cells and by which mechanisms do they integrate into prostatic buds? One possible origin is urethral intermediate or superficial epithelium (Abler et al., 2011a). The intermediate and superficial urethral epithelial layers (Keratin 14-) in i*Dnmt1*LOF mutants accumulate 5mC- cells similar to the core of prostatic buds. Intermediate and superficial epithelial cells could stream into prostatic bud cores while margin cells are extending prostatic bud axes by oriented cell division.

Given that DNMT1- cells can occupy the core of prostatic buds, it remains to be seen if this is a transient cell population or if they are retained in prostate tissue during glandular growth. Further studies are required to determine if DNMT1- cells from the bud core can contribute to the adult prostate or to the formation of glandular tissue in renal grafts. As DNMT- cells are replication impeded, we hypothesize that these cells would be eventually outcompeted by DNMT1 + cells during glandular growth. However, if there is a similar mechanism in normal tissues (where all bud cells express DNMT1) and cells in the core of prostatic buds derive from a distinct population than prostatic bud margins, it remains likely that these cells would participate in glandular development. It would require further investigation to determine whether cells from the bud core and margin give rise to phenotypically distinct epithelial populations within the mature prostate.

The existence of two distinct cell lineages within prostatic buds opens several new lines of investigation. Do characteristics and behaviors of these cells remain different into adulthood? Do both cell lineages possess or retain progenitor capacities and can they generate all prostatic epithelial cell types? The existence of multiple lineages in the urethral epithelium warrants further investigation using emerging techniques like single-cell RNA-sequencing to identify distinct cellular populations and to characterize progenitor cells. Further studies are required to follow these separate lineages into adulthood to determine how they contribute to the composition of the adult prostate.

5. Conclusions

We have established a requirement for urethral epithelial DNMT1 for prostatic bud formation and survival of early prostatic bud epithelial cells. Using *Dnmt1* ablation as a novel tool, we have identified that prostatic buds are elongated in part by oriented cell division, but that a unique cell lineage in prostatic bud cores arises by a proliferation independent mechanism.

Acknowledgements

We thank members of the Vezina laboratory for technical assistance, Dr. Robert Lipinski and Caden Ulschmid (University of Wisconsin-Madison) and Dr. Xin Sun (University of California, San Diego) for critical insights and Dr. Xin Sun for providing mice. We thank Scott Swanson and John Steill (Morgridge Institute) for help with RNA-Seq data submission. This work is supported by National Institutes of Health R01 DK099328, U54 DK104310 and U01 DK110807.

Appendix A. Supplementary material

Supplementary data associated with this article can be found in the online version at doi:10.1016/j.ydbio.2019.01.011.

References

Abler, L.L., Keil, K.P., Mehta, V., Joshi, P.S., Schmitz, C.T., Vezina, C.M., 2011a. A high-resolution molecular atlas of the fetal mouse lower urogenital tract. Dev. Dyn. 240, 2364–2377.

Abler, L.L., Mehta, V., Keil, K.P., Joshi, P.S., Flucus, C.L., Hardin, H.A., Schmitz, C.T., Vezina, C.M., 2011b. A high throughput in situ hybridization method to characterize mRNA expression patterns in the fetal mouse lower urogenital tract. J. Vis. Exp..

Agarwal, M.L., Agarwal, A., Taylor, W.R., Stark, G.R., 1995. p53 controls both the G2/M and the G1 cell cycle checkpoints and mediates reversible growth arrest in human fibroblasts. Proc. Natl. Acad. Sci. USA 92, 8493–8497.

Banin, S., Moyal, L., Shieh, S., Taya, Y., Anderson, C.W., Chessa, L., Smorodinsky, N.I., Prives, C., Reiss, Y., Shiloh, Y., Ziv, Y., 1998. Enhanced phosphorylation of p53 by ATM in response to DNA damage. Science 281, 1674–1677.

Bulut, H.E., Ozdemir, O., Basimoglu-Koca, Y., Korkmaz, M., Atalay, A., 1999. Effects of a DNA demethylating agent–5-azacytidine–on testicular morphology during mouse embryo development. Okajimas Folia Anat. Jpn. 76, 47–53.

Chen, T., Hevi, S., Gay, F., Tsujimoto, N., He, T., Zhang, B., Ueda, Y., Li, E., 2007. Complete inactivation of DNMT1 leads to mitotic catastrophe in human cancer cells. Nat. Genet. 39, 391–396.

Choi, J.-Y., Lee, S., Hwang, S., Jo, S.A., Kim, M., Kim, Y.J., Pang, M.-G., Jo, I., 2013. Histone H3 lysine 27 and 9 hypermethylation within the Bad promoter region mediates 5-Aza-2′-deoxycytidine-induced Leydig cell apoptosis: implications of 5-Aza-2′-deoxycytidine toxicity to male reproduction. Apoptosis 18, 99–109.

Cisneros, F.J., Branch, S., 2003. 5-AZA-2′-deoxycytidine (5-AZA-CdR): a demethylating agent affecting development and reproductive capacity. J. Appl. Toxicol. 23, 115–120.

Cunha, G.R., Baskin, L., 2016. Mesenchymal-epithelial interaction techniques. Differentiation 91, 20–27.

Elliott, E.N., Sheaffer, K.L., Schug, J., Stappenbeck, T.S., Kaestner, K.H., 2015. Dnmt1 is essential to maintain progenitors in the perinatal intestinal epithelium. Development 142, 2163–2172.

Feng, Y., Sentani, K., Wiese, A., Sands, E., Green, M., Bommer, G.T., Cho, K.R., Fearon, E.R., 2013. Sox9 induction, ectopic Paneth cells, and mitotic spindle axis defects in mouse colon adenomatous epithelium arising from conditional biallelic Apc inactivation. Am. J. Pathol. 183, 493–503.

Fischer, M., 2017. Census and evaluation of p53 target genes. Oncogene 36, 3943–3956.

Georgia, S., Kanji, M., Bhushan, A., 2013. DNMT1 represses p53 to maintain progenitor cell survival during pancreatic organogenesis. Genes Dev. 27, 372–377.

Grant, C.M., Kyprianou, N., 2013. Epithelial mesenchymal transition (EMT) in prostate growth and tumor progression. Transl. Androl. Urol. 2, 202–211.

Harfe, B.D., Scherz, P.J., Nissim, S., Tian, H., McMahon, A.P., Tabin, C.J., 2004. Evidence for an expansion-based temporal Shh gradient in specifying vertebrate digit identities. Cell 118, 517–528.

Hou, J., Charters, A.M., Lee, S.C., Zhao, Y., Wu, M.K., Jones, S.J., Marra, M.A., Hoodless, P.A., 2007. A systematic screen for genes expressed in definitive endoderm by serial analysis of gene expression (SAGE). BMC Dev. Biol. 7, 92.

Hou, Z., Jiang, P., Swanson, S.A., Elwell, A.L., Nguyen, B.K., Bolin, J.M., Stewart, R., Thomson, J.A., 2015. A cost-effective RNA sequencing protocol for large-scale gene expression studies. Sci. Rep. 5, 9570.

Jackson-Grusby, L., Beard, C., Possemato, R., Tudor, M., Fambrough, D., Csankovszki, G., Dausman, J., Lee, P., Wilson, C., Lander, E., Jaenisch, R., 2001. Loss of genomic methylation causes p53-dependent apoptosis and epigenetic deregulation. Nat. Genet. 27, 31–39.

Joseph, D.B., Chandrashekar, A.S., Abler, L.L., Chu, L.-F., Thomson, J.A., Mendelsohn, C., Vezina, C.M., 2018. In vivo replacement of damaged bladder urothelium by Wolffian duct epithelial cells. Proc. Natl. Acad. Sci. USA 115, 8394–8399.

Keil, K.P., Abler, L.L., Laporta, J., Altmann, H.M., Yang, B., Jarrard, D.F., Hernandez, L.L., Vezina, C.M., 2014a. Androgen receptor DNA methylation regulates the timing and androgen sensitivity of mouse prostate ductal development. Dev. Biol. 396, 237–245.

Keil, K.P., Abler, L.L., Mehta, V., Altmann, H.M., Laporta, J., Plisch, E.H., Suresh, M., Hernandez, L.L., Vezina, C.M., 2014b. DNA methylation of E-cadherin is a priming mechanism for prostate development. Dev. Biol. 387, 142–153.

Keil, K.P., Altmann, H.M., Mehta, V., Abler, L.L., Elton, E.A., Vezina, C.M., 2013. Catalog of mRNA expression patterns for DNA methylating and demethylating genes in developing mouse lower urinary tract. Gene Expr. Patterns 13, 413–424.

Keil, K.P., Mehta, V., Abler, L.L., Joshi, P.S., Schmitz, C.T., Vezina, C.M., 2012a. Visualization and quantification of mouse prostate development by in situ hybridization. Differentiation 84, 232–239.

Keil, K.P., Mehta, V., Branam, A.M., Abler, L.L., Buresh-Stiemke, R.A., Joshi, P.S., Schmitz, C.T., Marker, P.C., Vezina, C.M., 2012b. Wnt inhibitory factor 1 (Wif1) is regulated by androgens and enhances androgen-dependent prostate development. Endocrinology 153, 6091–6103.

Kurita, T., Medina, R.T., Mills, A.A., Cunha, G.R., 2004. Role of p63 and basal cells in the prostate. Development 131, 4955–4964.

Langmead, B., Trapnell, C., Pop, M., Salzberg, S.L., 2009. Ultrafast and memory-efficient alignment of short DNA sequences to the human genome. Genome Biol. 10, R25.

Li, B., Dewey, C.N., 2011. RSEM: accurate transcript quantification from RNA-Seq data with or without a reference genome. BMC Bioinform. 12, 323.

Li, E., Bestor, T.H., Jaenisch, R., 1992. Targeted mutation of the DNA methyltransferase gene results in embryonic lethality. Cell 69, 915–926.

Love, M.I., Huber, W., Anders, S., 2014. Moderated estimation of fold change and dispersion for RNA-seq data with DESeq. 2. Genome Biol. 15, 550.

Mehta, V., Abler, L.L., Keil, K.P., Schmitz, C.T., Joshi, P.S., Vezina, C.M., 2011. Atlas of Wnt and R-spondin gene expression in the developing male mouse lower urogenital tract. Dev. Dyn. 240, 2548–2560.

Mehta, V., Schmitz, C.T., Keil, K.P., Joshi, P.S., Abler, L.L., Lin, T.M., Taketo, M.M., Sun, X., Vezina, C.M., 2013. Beta-catenin (CTNNB1) induces Bmp expression in urogenital sinus epithelium and participates in prostatic bud initiation and patterning. Dev. Biol. 376, 125–135.

Monk, M., Boubelik, M., Lehnert, S., 1987. Temporal and regional changes in DNA methylation in the embryonic, extraembryonic and germ cell lineages during mouse embryo development. Development 99, 371–382.

Nasonkin, I.O., Merbs, S.L., Lazo, K., Oliver, V.F., Brooks, M., Patel, K., Enke, R.A., Nellissery, J., Jamrich, M., Le, Y.Z., Bharti, K., Fariss, R.N., Rachel, R.A., Zack, D.J., Rodriguez-Boulan, E.J., Swaroop, A., 2013. Conditional knockdown of DNA methyltransferase 1 reveals a key role of retinal pigment epithelium integrity in photoreceptor outer segment morphogenesis. Development 140, 1330–1341.

Niculescu, A.B., 3rd, Chen, X., Smeets, M., Hengst, L., Prives, C., Reed, S.I., 1998. Effects ofp21(Cip1/Waf1) at both the G1/S and the G2/M cell cycle transitions: pRb is a critical determinant in blocking DNA replication and in preventing endoreduplication. Mol. Cell. Biol. 18, 629–643.

Ozawa, K., 2008. Reduction of phosphorylated histone H3 serine 10 and serine 28 cell cycle marker intensities after DNA damage. Cytom. Part A: J. Int. Soc. Anal. Cytol. 73, 517–527.

Palii, S.S., Van Emburgh, B.O., Sankpal, U.T., Brown, K.D., Robertson, K.D., 2008. DNA methylation inhibitor 5-Aza-2′-deoxycytidine induces reversible genome-wide DNA damage that is distinctly influenced by DNA methyltransferases 1 and 3B. Mol. Cell. Biol. 28, 752–771.

Quick, C.M., Gokden, N., Sangoi, A.R., Brooks, J.D., McKenney, J.K., 2010. The distribution of PAX-2 immunoreactivity in the prostate gland, seminal vesicle, and ejaculatory duct: comparison with prostatic adenocarcinoma and discussion of prostatic zonal embryogenesis. Hum. Pathol. 41, 1145–1149.

Reik, W., Dean, W., Walter, J., 2001. Epigenetic reprogramming in mammalian development. Science 293, 1089–1093.

Seifert, A.W., Harfe, B.D., Cohn, M.J., 2008. Cell lineage analysis demonstrates an endodermal origin of the distal urethra and perineum. Dev. Biol. 318, 143–152.
Signoretti, S., Loda, M., 2006. Defining cell lineages in the prostate epithelium. Cell Cycle 5, 138–141.
Signoretti, S., Pires, M.M., Lindauer, M., Horner, J.W., Grisanzio, C., Dhar, S., Majumder, P., McKeon, F., Kantoff, P.W., Sellers, W.R., Loda, M., 2005. p63 regulates commitment to the prostate cell lineage. Proc. Natl. Acad. Sci. USA 102, 11355–11360.
Soriano, P., 1999. Generalized lacZ expression with the ROSA26 Cre reporter strain. Nat. Genet. 21, 70–71.
Srinivas, S., Watanabe, T., Lin, C.S., William, C.M., Tanabe, Y., Jessell, T.M., Costantini, F., 2001. Cre reporter strains produced by targeted insertion of EYFP and ECFP into the ROSA26 locus. BMC Dev. Biol. 1, 4.
Taube, J.H., Allton, K., Duncan, S.A., Shen, L., Barton, M.C., 2010. Foxa1 functions as a pioneer transcription factor at transposable elements to activate Afp during differentiation of embryonic stem cells. J. Biol. Chem. 285, 16135–16144.
Wang, J., Vasaikar, S., Shi, Z., Greer, M., Zhang, B., 2017. WebGestalt 2017: a more comprehensive, powerful, flexible and interactive gene set enrichment analysis toolkit. Nucleic Acids Res. 45, W130–W137.
Wozniak, R.J., Klimecki, W.T., Lau, S.S., Feinstein, Y., Futscher, B.W., 2007. 5-Aza-2′-deoxycytidine-mediated reductions in G9A histone methyltransferase and histone H3 K9 di-methylation levels are linked to tumor suppressor gene reactivation. Oncogene 26, 77–90.
Yuan, J.S., Reed, A., Chen, F., Stewart, C.N., 2006. Statistical analysis of real-time PCR data. BMC Bioinform. 7, 85.